Wet chemically synthesized optical investigation of Tb^{3+} activated $BaTiO_3$ phosphors for green emitting LEDs and display applications

R. B. AURADE[1], GAJANAN S. SOLANKE[2], ABHIJEET R. KADAM[1,*]
[1]*Department of Physics, CSMSS Chh. Shahu College of Engineering, Chhatrapati Sambhajinagar - 431011, India*
[2]*Department of Mathematics, CSMSS Chh. Shahu College of Engineering, Chhatrapati Sambhajinagar - 431011, India*

In the world of display technologies, lanthanide doped inorganic phosphors have become more popular in recent years. The suggested study uses a wet chemical approach to synthesize Tb^{3+}, doped $BaTiO_3$ phosphor. Phase Identification and vibrational features of proposed phosphor was confirmed using XRD and FTIR analysis. Under excitation at 351 nm, 368 nm, and 377 nm, the synthesized Tb^{3+} doped $BaTiO_3$ phosphors showed blue and green emission peak at 452 and 545 nm photoluminescence spectra (PL). The potential application of the produced phosphor in WLEDs alongside additional display applications is supported by all of those results.

(Received October 27, 2025; accepted April 6, 2026)

Keywords: Wet chemical, Lamp phosphor, LEDs

1. Introduction

Because of its wide range of applications, including as capacitors, electro optical systems, pyroelectric infrared sensors, ultrasonic transducers, positive temperature coefficient (PTC) resistors, and more, barium titanate ($BaTiO_3$) has been extensively investigated[1–4]. Its electrical properties can be effectively tailored through the use of different dopants and synthesis routes. The luminescence properties of $BaTiO_3$ nanopowders generated by different processes may also be significantly influenced by the nature and concentration of defects introduced during processing**.** Among the chemical elements utilized as dopants for $BaTiO_3$ are rare earths[3–6]. One of these, lanthanum, is a donor dopant that fills the Ba sites in the $BaTiO_3$ crystal lattice. When barium titanate ($BaTiO_3$) is doped with RE, it exhibits a shift in electrical resistance, particle size, and symmetry from tetragonal to cubic[9–11]. The $BaTiO_3$ structure becomes defective due to RE-doping, as it results in alterations to the A and B sites as well as an A-site vacancy. It follows that doping should have an impact on optical properties. It was demonstrated that the optical band gap value (derived from UV–Vis spectra) for RE-doped $BaTiO_3$ samples synthesized by solid state reaction reduced as La concentration increased. On doped samples, however, no broadening or shifting of the luminescence peaks is seen. However, it is known that the process of synthesis, which can result in the production of more or less structural flaws, might affect the physical properties (namely luminescence). There were several techniques utilized to prepare RE^{3+} doped $BaTiO_3$, including co-precipitation, spray pyrolysis, sol-gel, solid state reaction and the Pechini method, etc[7,10–15]. We want to investigate the effects of rare earth. In this context, the present work aims to investigate the influence of rare-earth doping on the luminescence characteristics of $BaTiO_3$ phosphors.

Rare earth ion luminescence in solids has previously been observed in recent decades[16–19]. Due to the unique electrical arrangement of rare earth elements, rare earth luminescent materials have numerous emission spectra due to the rich energy level structure of their 4f orbit. Rare earth polychromatic luminescence materials have drawn increasing attention in recent years from those working in the fields of displays, lighting, lasers, and photoelectric devices[20–23]. Tb^{3+} is a superior ion for activating green lights. $BaTiO_3$ is an attractive and relatively underexplored phosphor host due to its stable perovskite structure, defect-tolerant lattice, and ability to accommodate rare-earth ions through charge compensation mechanisms**.** In addition to its well-known dielectric and ferroelectric properties, $BaTiO_3$ provides a robust crystal environment that supports efficient rare-earth emission by suppressing non-radiative relaxation**,** making it a promising multifunctional host for luminescent and display applications. In light of the aforementioned, Tb^{3+}-doped $BaTiO_3$ microcrystals were synthesized in the present work using a wet chemical route. The structural properties were examined using X-ray diffraction (XRD) and Fourier transform infrared (FTIR) spectroscopy. Photoluminescence (PL) studies were carried out to confirm the luminescent characteristics of Tb^{3+}-activated $BaTiO_3$ and to evaluate its potential for display device applications[24–26].

2. Synthesis and characterizations

The $BaTiO_3$ phosphors Tb^{3+} doped phosphor samples were synthesized by wet chemical synthesis. In a distinctive synthesis method, specific amounts of $Ba(NO_3)_2.4H_2O$ and

TiO_2 were mixed. Tb_4O_7 (99.99 %) were dissolved in nitric acid to convert them into nitrates. and all reagents were dissolved in a small quantity of double-distilled water. The solution is then heated to 85 ºC in a water bath while being constantly stirred to produce a homogenous precipitate. This Precipitate is dried in hot air oven over the night and sample was collected. The dried powder was then gently ground for 5 min and used for further characterization**.s**

The produced $BaTiO_3$ phosphor's phase purity was assessed using a number of analytical methods. The RIGAKU mini flex 600 XRD apparatus was used to investigate the powder patterns from XRD that were acquired using Cu Kα radiation (λ = 1.5405 Å). The vibrational properties of the material were examined using Fourier transform infrared spectroscopy (FTIR). We performed photoluminescence (PL) experiments, including excitation and emission spectra, to further characterize the material. The SHIMADZU spectrofluorophotometer RF 5301 was used to perform these measurements.

3. Result and discussion

3.1. XRD analysis

Step scanning at intervals of 0.02° was used to monitor the XRD pattern of the synthesized $Ba_{1-x}TiO_3$: Tb^{3+}, phosphor in the range of (20−80°), as shown in Fig. 1. The detected diffraction peaks are in good agreement with JCPDS card number 82-1175. The peaks are thin, clear, and distinct, suggesting that the diffraction pattern is clearly indexed. The existence of these peaks is explained by the possibility that rare earth ions, whose ionic radii are similar to those of Ba^{2+}, will occupy these interstitial positions. The near ionic radius match between Ba^{2+} ions and rare earths explains this substitution. The close agreement with the standard JCPDS data confirms that the phosphor samples were successfully synthesized with high phase purity.

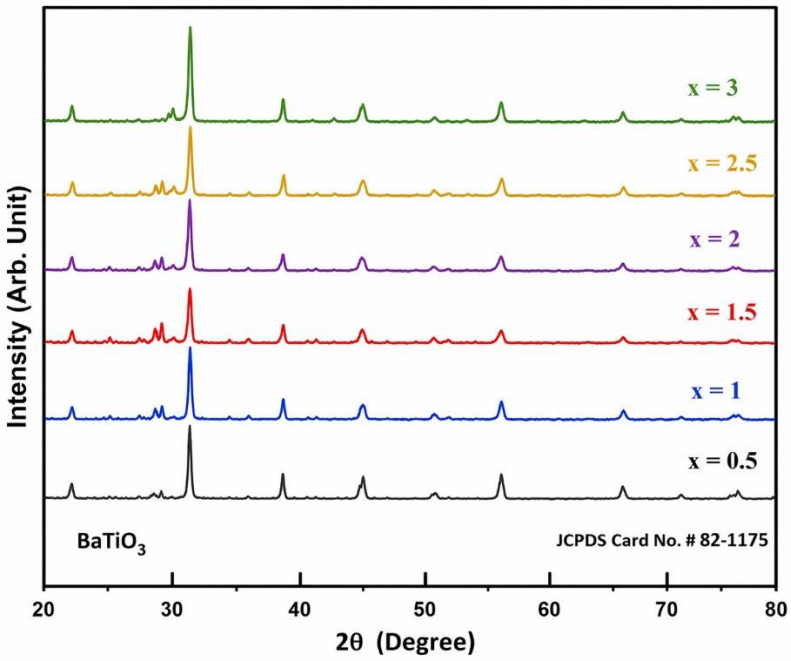

Fig. 1. XRD analysis of $Ba_{1-x}TiO_3$:xTb^{3+} phosphors (colour online)

3.2. FTIR analysis

The $BaTiO_3$ perovskite phosphor's FT-IR illustrations are displayed in Fig. 2. The common explanation for the band at 1421 cm^{-1} is the asymmetric stretching vibration of carbonate groups. The carbonate groups' symmetric stretching vibration is correlated with the absorption at 1003 cm^{-1}. This peak provides additional evidence that carbonate ions are present in the sample. The carbonate group's out-of-plane bending vibration is linked to the band at 696 cm^{-1}. The recognition of carbonate ions in the material is also supported by this vibration mode. The presence of the Ti–O stretching vibration band at 553 cm^{-1} in the FT−IR spectra, which is compatible with the findings from other analytical techniques like XRD, strongly supports the establishment of the perovskite structure in the prepared material. The effective synthesis of the desired perovskite phase is confirmed by this validation. The characteristic Ti–O stretching vibrations in the infrared spectra of $BaTiO_3$ are well-known. The absorption peak located at 560 cm^{-1} is indicative of the particular vibration mode of the Ti–O bonds seen in the $BaTiO_3$ structure. In the FT-IR spectra, the absorption bands at wave numbers (723 and 772) cm^{-1} are linked to metal–oxygen (M−O) vibrations, specifically with the bonds between titanium and oxygen (Ti–O) and titanium and oxygen–titanium (Ti–O–Ti)[3,27–29].

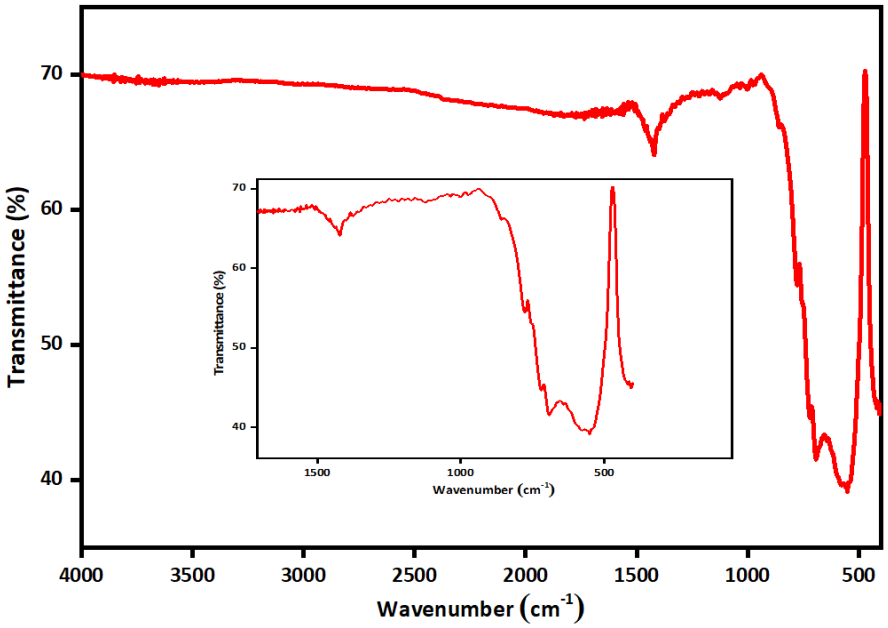

Fig. 2. FTIR analysis of $BaTiO_3$ phosphor (colour online)

3.3. Photoluminescence investigation

On doping Tb^{3+} ions, PL emission and excitation spectra were observed for the identical host lattice. The PL excitation spectrum exhibits several peaks in the near-ultraviolet (NUV) region, with prominent peak positions at 351, 368, and 377 nm. The $^7F_6 \rightarrow {}^5L_9$ transitions are responsible for the peaks at 351 and 368 nm, whereas the $^7F_6 \rightarrow {}^5D_3$ transition shown in Fig. 3 is responsible for the peak at 377 nm[32,33]. The two wavelengths at which the peaks at 351 and 377 nm are the most influential are those at which we record PL emission spectra. Two strong emission peaks were found at 452 and 545 nm, along with a few smaller, more broadly orientated peaks at 452 and 488 the wavelengths. The emission peaks at 452 and 488 nm arise from the $^5D_4 \rightarrow {}^7F_6$ transitions, whereas the strong green emission at 545 nm is assigned to the $^5D_4 \rightarrow {}^7F_5$ transition, as illustrated in Figs. 4 and 5 [34–37].

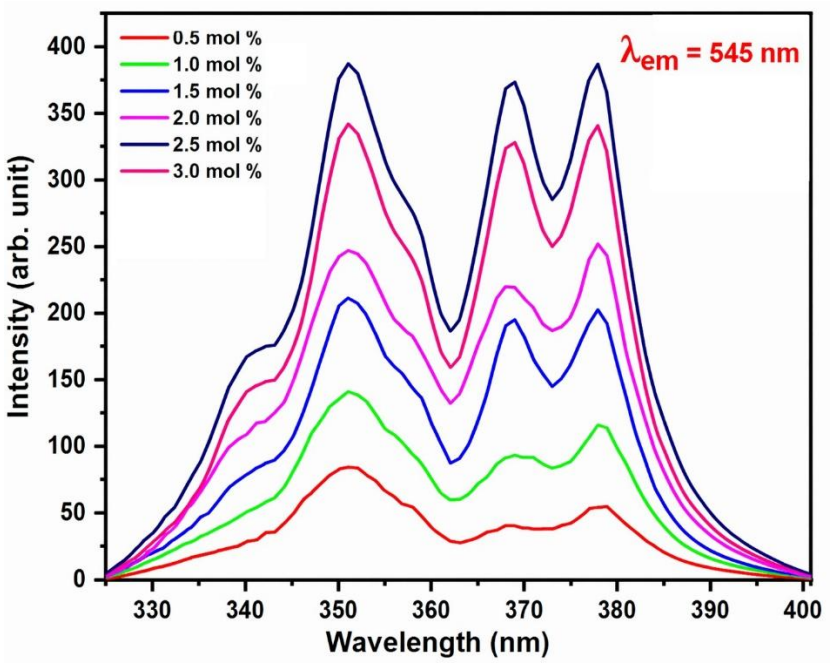

Fig. 3. PL excitation spectra of $BaTiO_3$:xTb^{3+} phosphor monitored at emission of 545 nm (colour online)

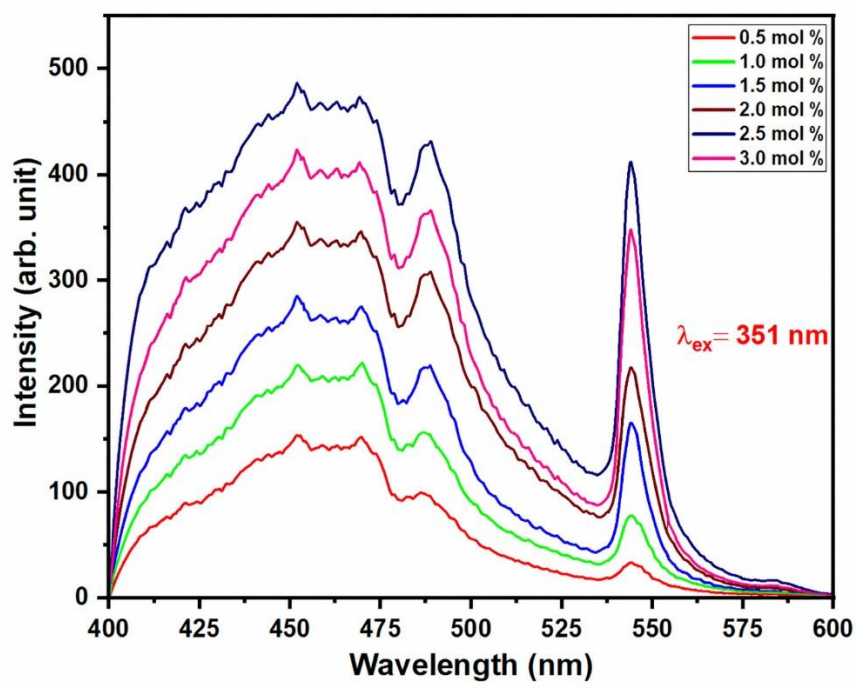

Fig. 4. PL emission spectra of $BaTiO_3$:xTb^{3+} phosphor at excitation of 351 nm (colour online)

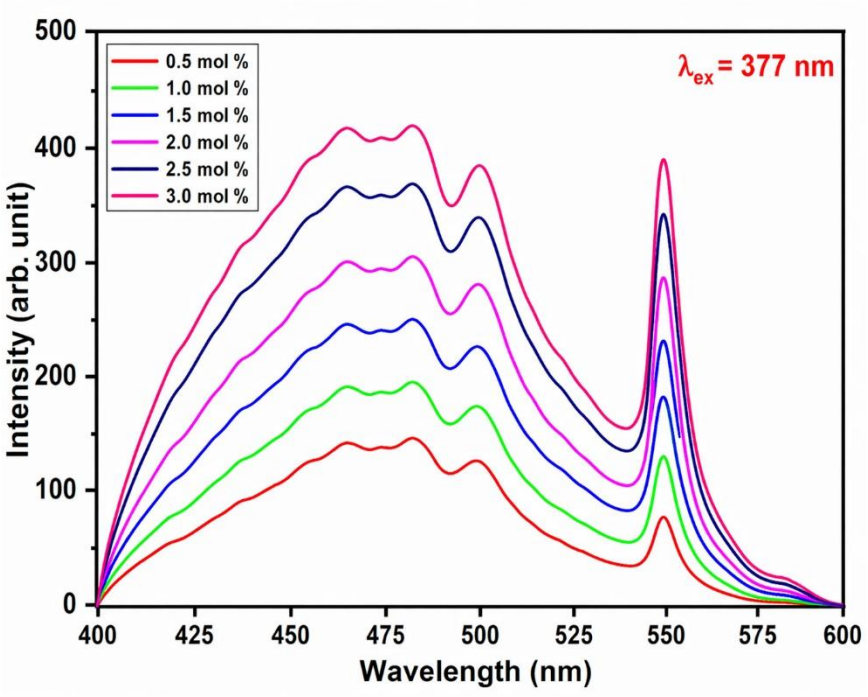

Fig. 5. PL emission spectra of $BaTiO_3$:xTb^{3+} phosphor at excitation of 377 nm (colour online)

Additionally, the Tb^{3+} activated $BaTiO_3$ phosphor's intensity increases with concentration up to 2.5%, after which it decreases. The quenching effect of concentration is the cause of this intensity drop. At critical concentration (X_C), the critical transfer distance (R_C) between the host ligand and activator ion is the nearby distance that causes the concentration quenching effect. The concentration quenching effect's accountable interaction will be determined by the value of R_C. The mechanism of exchange interactions is in charge of the decrease in concentration intensity if R_C is less than 5. Multipolar interaction is responsible for the same if it exceeds 5. The Blasse theory determines the critical transfer distance [20,38–40]

$$R_C = 2\left(\frac{3V}{4\prod X_C N}\right)^{1/3} \quad (1)$$

The ideal concentrations for Tb^{3+} is Xc = 2.5 mol%, and N = 2 is the number of cations in the unit cell, assuming that V = 196.90 $Å^3$ is the unit cell's volume. For Tb^{3+} ions, the formula now states that R_C equals 4.22. Thus, in Tb^{3+} doped $BaTiO_3$ phosphors, the concentration quenching effect is caused by exchange interaction.

As per the Van Uitert's theory interactions responsible for the concentration quenching in Tb^{3+} doped $BaTiO_3$ phosphors [34,35]

$$\frac{I}{x} = k[1 + \beta.x^{\frac{\theta}{3}}]^{-1} \qquad (2)$$

In this case, x stands for the doping concentration, k and β are constants, and I stand for the lanthanide triggered phosphor intensity. The type of interaction that causes concentration quenching is dependent on the value of θ, as per the Van Uitert theory, which is based on the previously mentioned research[36]. Relation between log (x) and log (I/x) are depicted in Fig.6 for Tb^{3+} doped $BaTiO_3$ phosphors[37–39]. Slope of given linear fits for the Tb^{3+} doped $BaTiO_3$ phosphors are -0.0389. Therefore, values of θ are 0.1167 for Tb^{3+} which are nearly equal to 3 therefore exchange interaction is responsible for the concentration quenching for Tb^{3+} ions.

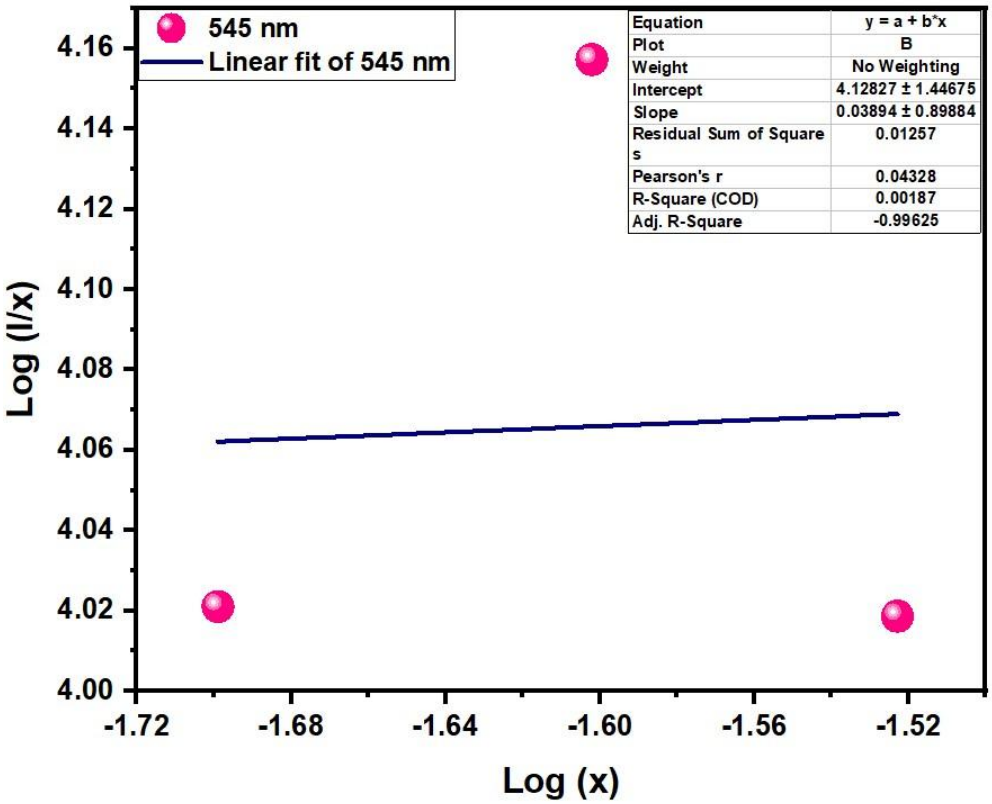

Fig. 6. Log(x) Vs Log(I/x) for Tb^{3+} doped $BaTiO_3$ phosphors (colour online)

3.4. CIE photochromaticity

Fig. 7 displays the chromaticity coordinates of $BaTiO_3$: Tb^{3+} phosphor, which were established by the Commission de I Eclairage (CIE)[42]. (0.2910, 0.6773) are the colour coordinates of $BaTiO_3$ phosphors. These¬ phosphors show green light, as seen in Fig.7. The given formula determines the colour purity of the suggested sample[35,39–48];

$$Color\ purity = \frac{\sqrt{(X-X_i)^2+(Y-Y_i)^2}}{\sqrt{(X_d-X_i)^2+(Y_d-Y_i)^2}} 100\ \% \qquad (3)$$

where X_i and Y_i are the coordinates of white light (0.333, 0.333), X_d and Y_d are the dominant coordinates of proposed phosphor (0.266, 0.666) and X and Y are the CIE color coordinates of proposed phosphor. Hence the color purity of proposed phosphor is found to be 90.24 %.

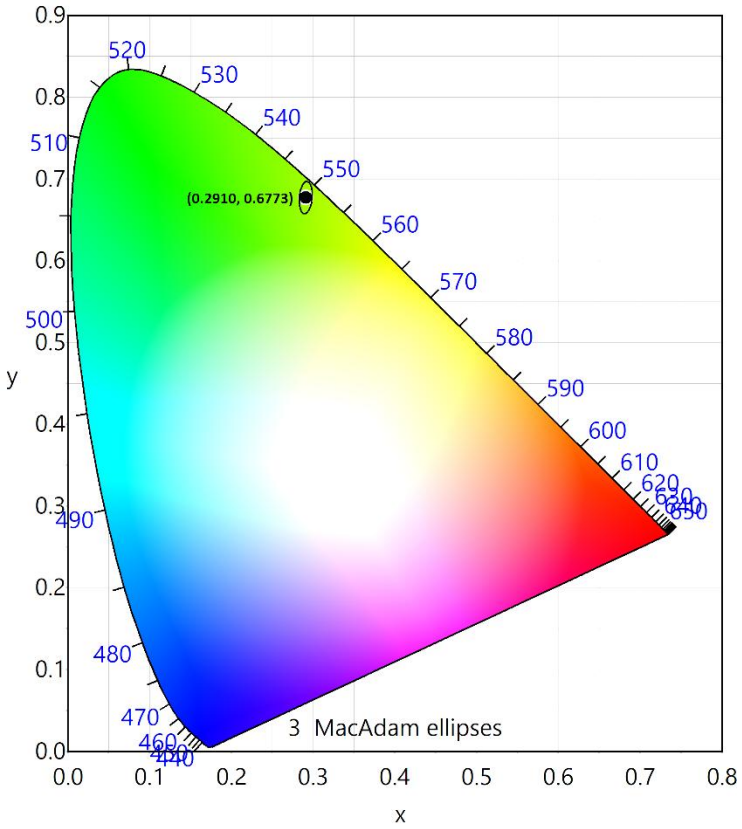

Fig. 7. CIE chromaticity of 2.5 mol % Tb^{3+} activated $BaTiO_3$ phosphors (colour online)

4. Conclusion

The present study employs a wet chemical route to synthesize Tb^{3+}-doped $BaTiO_3$ phosphors**,** which facilitates charge compensation effects and influences the photochromic behavior of Tb^{3+} ions**.** Various characterization techniques were employed to confirm the formation and properties of the synthesized phosphors. The crystalline structure and vibrational features were examined using X-ray diffraction (XRD) and Fourier transform infrared (FTIR) spectroscopy, respectively. The optical properties of the phosphor exhibit strong emission in the green region. The calculated CIE color purity of the phosphor is 90.24%. Overall, the phosphor demonstrates promising potential as a green-emitting material for WLEDs and displays devices applications.

References

[1] D.S. Smith, N. Ghayoub, I. Charissou, O. Bellon, P. Abélard, A.H. Edwards, J. Am. Ceram. Soc. **81**, 1789 (1998).
[2] J. Liu, S. Gong, L. Quan, B. Chen, D. Zhou, J. Am. Ceram. Soc. **95**, 1640 (2012).
[3] V. Singh, A. Nande, A. A. Bhat, S. J. Dhoble, S. Watanabe, T. K. Gundu Rao, Ceram. Int. **51**, 30896 (2025).
[4] M. H. Taywade, Y. R. Parauha, N. S. Dhoble, S. J. Dhoble, Mater. Res. Bull. **197**, 113985 (2026).
[5] A. E. Souza, S. R. Teixeira, C. M. -Santos, W. H. Schreiner, P. N. Lisboa Filho, E. Longo, J. Mater. Chem. C **2**, 7056 (2014).
[6] A. C. Ianculescu, C. A. Vasilescu, M. Crisan, M. Raileanu, B. S. Vasile, M. Calugaru, D. Crisan, N. Dragan, L. Curecheriu, L. Mitoseriu, Mater. Charact. **106**, 195 (2015).
[7] S. Fuentes, R. Espinoza-González, M. Rosales, J. León, J. Alloys Compd. **846**, 156452 (2020).
[8] A. Patra, C. S. Friend, R. Kapoor, P. N. Prasad, Chem. Mater. **15**, 3650 (2003).
[9] A. Rached, M. A. Wederni, K. Khirouni, S. Alaya, R. J. Martín-Palma, J. Dhahri, Mater. Chem. Phys. **267**, 124600 (2021).
[10] M. Borah, D. Mohanta, Appl. Phys. A Mater. Sci. Process. **115**, 1057 (2014).
[11] M. Cernea, M. Secu, R. Radu, P. Ganea, V. A. Surdu, R. Trusca, E. T. Vasile, E. C. Secu, J. Alloys Compd. **878**, 160380 (2021).
[12] W. Li, Z. Xu, R. Chu, P. Fu, J. Hao, J. Alloys Compd. **482**, 137 (2009)
[13] C. Zhu, Q. Zhao, Z. Cai, L. Guo, L. Li, X. Wang, J. Alloys Compd. **829**, 154496 (2020).
[14] H. Jena, K. V. G. Kutty, T. R. N. Kutty, Mater. Res. Bull. **39**, 489 (2004).
[15] S. K. Lee, T. J. Park, G. J. Choi, K. K. Koo, S.W. Kim, Mater. Chem. Phys. **82**, 742 (2003).
[16] V. Sebastian, Magnetoelectric Polymer-Based Composites: Fundamentals and Applications, Senentxu Lanceros-Méndez, Pedro Martins (eds.), John Wiley & Sons Inc., 125 (2017).
[17] B. D. Stojanovic, A. S. Dzunuzovic, N. I. Ilic,

Magnetic, Ferroelectric, and Multiferroic Metal Oxides, Elsevier Inc., 333 (2018).
[18] S. R. Bhelave, A. R. Kadam, A. N. Yerpude, S. J. Dhoble, Luminescence **38**(4), 379 (2023).
[19] R. V Tikale, A. R. Kadam, S. J. Dhoble, Chem. Data Collect. **40**, 100891 (2022).
[20] R. G. Deshmukh, A. R. Kadam, S. J. Dhoble, J. Mol. Struct. **1257**, 132603 (2022).
[21] P. N. Parale, A. R. Kadam, K. V. Dabre, S. J. Dhoble, Mater. Lett. X **18**, 100191 (2023).
[22] S. Som, P. Mitra, V. Kumar, V. Kumar, J. J. Terblans, H. C. Swart, S. K. Sharma, Dalton Transactions **43**, 9860 (2014).
[23] G. Gu, W. Xiang, C. Yang, X. Liang, CrystEngComm **17**, 4554 (2015).
[24] X. Yuan Sun, S. Ming Huang, X. San Gong, Q. Chun Gao, Z. Piao Ye, C. Yan Cao, J. Non. Cryst. Solids **356**, 98 (2010).
[25] Y. V. Baklanova, L. G. Maksimova, O. A. Lipina, A. P. Tyutyunnik, V. G. Zubkov, J. Lumin. **224**, 117315 (2020).
[26] X. Liu, X. Chen, Y. Yu, W. Xie, Y. Zhao, S. Luo, G. Mei, J. Lin, Inorg. Chem. **59**, 12348 (2020).
[27] A. U. Trápala-Ramírez, J. L. N. Gálvez-Sandoval, A. Lira, I. Camarillo, E. Alvarez-Ramos, A. N. Meza-Rocha, U. Caldiño, J. Lumin. **215**, 116621 (2019).
[28] P. N. Parale, A. R. Kadam, S. J. Dhoble, K. V. Dabre, RSC Adv. **13**, 26179 (2023).
[29] R. S. Yadav, Monika, E. Rai, L. P. Purohit, S. B. Rai, J. Lumin. **217**, 116810 (2020).
[30] U. Ahmed, M. M. Shahid, S. Shahabuddin, N. A. Rahim, M. Alizadeh, A. K. Pandey, S. Sagadevan, J. Alloys Compd. **860**, 158228 (2021).
[31] A. R. Kadam, G. C. Mishra, S. J. Dhoble, J. Mol. Struct. **1225**, 129129 (2021).
[32] H. Liu, L. Mei, L. Liao, Y. Zhang, Q. Guo, T. Zhou, Y. Wang, L. Li, J. Alloys Compd. **770**, 1237 (2019).
[33] M. R. Pansare, G. S. Solanke, A. R. Kadam, J. Electron. Mater. **55**, 3068 (2026).
[34] J. Zhou, Z. Xia, J. Mater. Chem. C **3**, 7552 (2015)
[35] Z. Yahiaoui, M. A. Hassairi, M. Dammak, E. Cavalli, F. Mezzadri, J. Lumin. **194**, 96 (2018).
[36] K. Dubey, A.R. Kadam, N. Baig, N. S. Dhoble, S. J. Dhoble, Radiation Effects and Defects in Solids **176**(5-6), 431 (2021).
[37] A. R. Kadam, R. B. Aurade, S. J. Dhoble, J. Alloys Compd. **1057**, 186709 (2026).
[38] P. N. Parale, A. R. Kadam, N. S. Shirbhate, S. J. Dhoble, K. V. Dabre, J. Fluoresc. **35**, 6035 (2025).
[39] E. Ansari, S. K. Patle, N. S. Ugemuge, A. R. Kadam, S. J. Dhoble, J. Mol. Struct. **1349**, 143856 (2026).
[40] R. V. Tikale, A. D. Koparkar, A. R. Kadam, S. J. Dhoble, J. Fluoresc. **35**, 7771 (2025).
[41] A. R. Kadam, S. J. Dhoble, J. Alloys Compd. **884**, 161138 (2021).
[42] T. S. Dhapodkar, A. R. Kadam, N. Brahme, S. J. Dhoble, Mater. Today Chem. **24**, 100938 (2022).
[43] W. Zhang, R. Zhang, S. Yang, R. Wang, L. Na, R. Hua, Mater. Res. Bull. **122**, 110689 (2020).
[44] J. Papan, D. Jovanović, M. Sekulić, E. Glais, M. D. Dramićanin, Powder Technol. **346**, 150 (2019).
[45] V. Singh, A. R. Kadam, S. J. Dhoble, H. Jeong, Optik **243**, 167327 (2021).
[46] A. R. Kadam, G. C. Mishra, A. D. Deshmukh, S. J. Dhoble, J. Lumin. **229**, 117676 (2021).
[47] A. R. Kadam, S. B. Dhoble, G. C. Mishra, A. D. Deshmukh, S. J. Dhoble, J. Mol. Struct. **1233**, 130150 (2021).
[48] S. G. M. Mushtaque, A. R. Kadam, S. J. Dhoble, J. Mol. Struct. **1274**, 134510 (2023).

*Corresponding author: arkadam6@gmail.com